A Clamped IPT System With Adaptive Mode Switching Against Large Coupling Variations

Bin Yang, *Student Member, IEEE*, Binshan Zhang, Zeheng Zhang, Ying Luo, Ruikun Mai, *Senior Member, IEEE*, Zhengyou He, *Senior Member, IEEE*, and Yang Chen, *Member, IEEE*

***Abstract*—Misalignment issue is almost inevitable in an inductive power transfer (IPT) system, leading to unstable power transfer due to the coupling variations. In order to improve the flexibility of the IPT system, the misalignment range of stable power output is desired to be as large as possible. This article proposes a clamped IPT system to improve antimisalignment ability based on the dual-mode operation. The clamped circuit is constructed with a coil and a rectifier connected to the input dc terminal of the inverter. With the effect of the clamped circuit, the operating mode of the system can be adaptively switched to match the required coupling variation region without coupling identification, output detection, or feedback communication. Then, the analysis and parametric design of the system are elaborated. Finally, a 480-W experimental setup was built to verify the feasibility of the proposed method. Experimental results show that the proposed method can maintain stable output power between 440 and 480 W with the coupling varying from 0.14 to 0.39, while the efficiency is from 83.22% to 93.55%.**

***Index Terms*—Clamped circuit, coupling variation, inductive power transfer (IPT), parameters design, stable power transfer.**

I. Introduction

CURRENTLY, the inductive power transfer (IPT) technique has been used in many applications due to its attractive advantages, such as flexibility, convenience, safety, and user-friendliness. As one of the key indicators to evaluate system reliability, the misalignment tolerance ability of the IPT system has drawn much attention from researchers.

To restrain the fluctuation of the power, a common method is to introduce a control strategy into the IPT system so that the dc-dc converter, full-bridge inverter, and active rectifier can realize the desired misalignment insensitive output [1], [2], [3]. Besides, a variable inductor is proposed to keep the output stable versus misalignment [4], [5]. However, the controller may suffer from an extensive range of modulation depth with a large coupling variation, resulting in a decline in stability and efficiency [6]. Moreover, multivariable control strategies are proposed to improve the antimisalignment performance [7]. However, more control variables increase the system's complexity. Although the control strategy is an effective and active approach to addressing the misalignment problem, output detection and wireless communication are required.

In order to simplify the complexity of the system, many researchers have advocated improving misalignment tolerance by employing the inherent characteristic of the IPT system, including the design of coils [8], [9], [10] and topologies [11], [12], [13], [14], [15], [16], [17], [18], [19], [20], [21], [22]. For the design of coils, many magnetic couplers are proposed to stabilize the system output when misalignment occurs, such as the asymmetric coil [8], three-coil structure [9], and double-D coil [10]. The principle of coils design is to maintain the coupling coefficient stable so that the misalignment ability of the system is improved in one or two directions.

As an alternative solution, topology design methods are proposed, including hybrid topologies, and detuned topologies. The concept of hybrid topology was previously introduced by Zhao et al. [11]. With the interaction of two topologies with opposite output trends to pad misalignment, the total transfer power can maintain relatively constant. Similar approaches were proposed and expanded in [12] and [13]. Furthermore, Qu et al. [14] construct a family of hybrid topologies and synthetically analyze the design principles and characteristics for all hybrid topology systems. Usually, the hybrid topologies formed by LCC-LCC and S-S topologies [11] or S-LCC and LCC-S topologies [12] are employed to achieve a higher misalignment tolerance. Since the unique feature of merging with two compensation topologies, the complexity and high cost are inevitable. By contrast, the detuned circuit is simpler. Through the special design of compensation parameters, the primary current can be adaptively adjusted to obtain stable transfer power versus the coupling variation. There are a lot of works recording the antimisalignment performance of different detuned circuits. And a series of high-order compensation topologies with optimized parameters are proposed to ensure high misalignment tolerance, such as S-S [7], S-SP [15], LCC-S [16], S-CLC [17], double-T [18], and X-type topology [19]. Besides, a family of compensation topologies with secondary parallel compensation is proven to have strong misalignment tolerances [20]. However, the allowable coupling variation of this method needs to be further developed.

As we know, the profile of transfer power versus coupling variation (*P-k* profile) is determined once the parameters of the

Manuscript received 2 January 2023; revised 12 March 2023; accepted 22 May 2023. Date of publication 6 June 2023; date of current version 28 July 2023. This work was supported in part by the National Natural Science Foundation of China under Grant 52207226, and in part by the Sichuan Science and Technology Program under Grants 2023NSFSC0819 and 2023JDRC0102. Recommended for publication by Associate Editor C. Lee. *(Corresponding author: Yang Chen.)*

The authors are with the School of Electrical Engineering, Southwest Jiaotong University, Chengdu 611756, China (e-mail: yb@my.swjtu.edu.cn; zbs@my.swjtu.edu.cn; hengs@my.swjtu.edu.cn; 2395420301@qq.com; mairk@swjtu.edu.cn; hezy@home.swjtu.edu.cn; yangchen@swjtu.edu.cn).

Color versions of one or more figures in this article are available at https://doi.org/10.1109/TPEL.2023.3283421.

Digital Object Identifier 10.1109/TPEL.2023.3283421

circuit are designed. To extend the misalignment distance, the reconfigurable IPT system with multimode operation is proposed [21], [22], [23], [24]. With the assistance of extra coils or reactive elements with active switching devices, the circuit structure can be changed to adjust the *P-k* profile so that the desired output power can be obtained within a larger coupling range. A detuned reconfigurable topology is proposed in [21], which utilizes a switch to convert between the detuned LCC-S topology and the detuned S-S topology so that stable power can be obtained within the coupling range of (0.1–0.25). In [22], a reconfigurable resonant coil is employed to widen the range of coupling based on the complementary power profile of different coils. Besides, a reconfigurable topology combining the S-S and LCCC-S topologies is proposed to enhance power transfer capability and tolerate weak couplings [23]. Moreover, a reconfigurable rectifier-based detuned S-S compensated IPT system is proposed to tolerate an extensive coupling [24]. Although stable power transfer is achieved chiefly, accurate coupling identification (or output detection) and feedback communication are required, increasing control circuit complexity and reducing the system reliability. If the system can match the operation mode adaptively according to the coupling, the system's reliability, ruggedness, and applicability will be further enhanced.

In the past, the diode clamping circuit has attracted the attention of some scholars due to its adaptive on-and-off characteristics. In [25], a half-bridge CLC-S IPT system with clamping diodes is used for primary coil disconnection protection, soft-start, and short-circuit protection. Moreover, The IPT system with primary [26] and secondary [27] diode clamping circuit were proposed to adaptively regulate the operation mode for battery charging. However, these methods are only proposed on the condition of a fixed coupling coefficient.

To address the above-mentioned issue, a clamped IPT system is proposed to enhance the misalignment tolerance in this article. With the assistance of the primary clamp circuit, the operation modes of the system can adaptively alter from one to the other without detection or feedback communication devices. Besides, a parameter design method taking account of dual-mode is proposed to maintain stable power output in the misalignment case. With the cooperation of different operation modes, the system can obtain a strong antimisalignment capacity.

The rest of this article is organized as follows. The analysis of the clamped IPT system is described in Section II. A parametric design criterion is presented in Section III. In Section IV, a 480 W prototype was constructed to verify the theoretical analysis. Finally, the conclusion is drawn in Section V.

II. Theoretical Analysis

The proposed clamped IPT system is shown in Fig. 1, consisting of a power input loop, a power output loop, and a clamp loop. The corresponding current is expressed in each loop by I_p, I_s, and I_c, respectively. X_p, X_s, and X_c are the equivalent reactance of each loop, which are given as follows:

$$\begin{cases} X_p = \omega L_{cp} + \omega L_p - 1/\omega C_p \\ X_s = \omega L_s - 1/\omega C_s \\ X_c = \omega L_{cc} - 1/\omega C_c \end{cases} \tag{1}$$

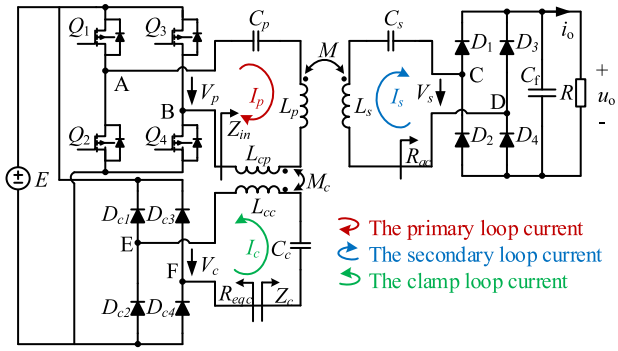

Fig. 1. Clamped IPT system.

where ω is the angular frequency, C_p, C_s, and C_c are the compensation capacitor of each loop, L_p (L_{cp}) and L_s (L_{cc}) are the self-inductances of the loosely coupled transformer (clamp transformer). And C_s is used to compensate the self-inductance L_s fully, i.e., $X_s = 0$.

E is the input dc voltage of the inverter ($Q_{p1} - Q_{p4}$) and the output dc voltage of the rectifier ($D_{c1} - D_{c4}$). V_p is the output ac voltage of the inverter ($Q_{p1} - Q_{p4}$). V_s (R_{ac}) and V_c (R_{eqc}) are used to represent the ac input voltage (the equivalent ac loads) of the rectifier constituted by ($D_{s1} - D_{s4}$) and ($D_{c1} - D_{c4}$). Z_c is the output impedance of the system reflected in the clamped circuit. R is the dc load of the rectifier ($D_{s1} - D_{s4}$). According to Kirchhoff's voltage law, the system can be described as follows:

$$\begin{cases} V_p = jX_pI_p - j\omega MI_s + j\omega M_cI_c \\ V_s = R_{ac}I_s = j\omega MI_p - jX_sI_s \\ V_c = R_{eqc}I_c = j\omega M_cI_p + jX_cI_c \end{cases} \tag{2}$$

where M (M_c) is the mutual inductance of the loosely coupled transformer (clamp transformer), which can be expressed by $M = k\sqrt{L_pL_s}$ and k represents the coupling coefficient of the loosely coupled transformer.

The relationship between E and V_p, R and R_{ac} can be expressed as follows [21]:

$$E = V_p\sqrt{2}\pi/4, R_{ac} = 8R/\pi^2. \tag{3}$$

For the clamped loop, there are three operation modes [26]: the turned-OFF mode, the partly activated mode, and the fully active mode. The analysis of the different modes is given as follows.

A. Analysis of Turned-Off or Partly Activated Mode

Assumed that the clamped loop is turned OFF, the rectifier bridge ($D_{c1} - D_{c4}$) cannot be conducted, and the current I_c in the clamp loop will be considered as zero, as follows:

$$I_c = 0\left(\sqrt{2}\,|V_c| \le E\right). \tag{4}$$

In this case, the system can be considered as a detuned S-S topology, as Fig. 2. Then, (2) can be described as follows:

$$\begin{cases} V_p = jX_pI_p - j\omega MI_s \\ 0 = -j\omega MI_p + R_{ac}I_s + jX_sI_s \end{cases}. \tag{5}$$

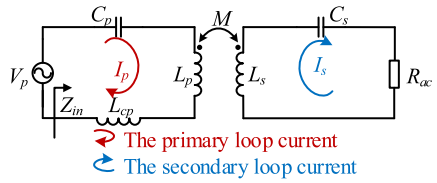

Fig. 2. Detuned S-S topology.

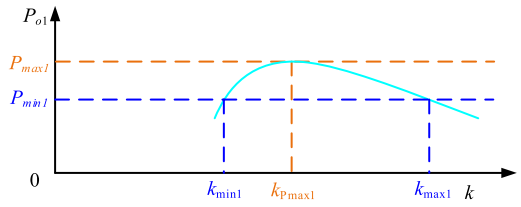

Fig. 3. Curve of the output power P_{o1} in the turned-OFF or partly activated mode, where $P_{\max 1}$ is the maximum output power, k_{pmax1} is the corresponding coupling coefficient, $P_{\min 1}$ is presumed minimum output power, and the corresponding couplings are $k_{\min 1}$ and $k_{\max 1}$.

Substituting $X_s = 0$ and (4) into (5), I_p and I_s can be obtained as follows:

$$\begin{cases} I_p = \frac{V_p R_{ac}\left(L_p L_s \omega^2 k^2 - j X_p R_{ac}\right)}{X_p^2 R_{ac}^2 + L_p^2 L_s^2 \omega^4 k^4} \\ I_s = \frac{V_p \sqrt{L_p L_s}\omega k\left(X_p R_{ac} + j L_p L_s \omega^2 k^2\right)}{X_p^2 R_{ac}^2 + L_p^2 L_s^2 \omega^4 k^4} \end{cases}. \tag{6}$$

From (6), the input impedance Z_{in} and the input impedance angle θ can be derived as follows:

$$\begin{cases} Z_{in} = \frac{V_p}{I_p} = \frac{L_p L_s \omega^2 k^2}{R_{ac}} + j X_p \\ \theta = \arctan\left(\frac{X_p R_{ac}}{L_p L_s \omega^2 k^2}\right) \end{cases}. \tag{7}$$

Moreover, the output power P_{o1} can be calculated as (8), which can be viewed as a function of the coupling k, and the corresponding curve is depicted in Fig. 3.

$$P_{o1}(k) = |I_s|^2 R_{ac} = \frac{V_p^2 R_{ac} \omega^2 L_p L_s k^2}{X_p^2 R_{ac}^2 + L_p^2 L_s^2 \omega^4 k^4}. \tag{8}$$

Setting the derivative of P_{o1} to zero, i.e., $dP_{o1}/dk = 0$, the coupling coefficient k_{pmax1} corresponding to the maximum output power $P_{\max 1}$ can be solved as follows:

$$k_{\mathrm{p\ max\ 1}} = \sqrt{\frac{X_p R_{ac}}{\omega^2 L_p L_s}}. \tag{9}$$

Substituting (9) into (8), the maximum output power $P_{\max 1}$ can be given as follows:

$$P_{\max 1} = \frac{V_p^2}{2 X_p}. \tag{10}$$

Then, the presumed minimum output power $P_{\min 1}$ satisfies

$$P_{\min 1} = P_{o1}(k_{\min 1}) = P_{o1}(k_{\max 1}). \tag{11}$$

A variable β is defined to describe the power fluctuation, i.e.,

$$\beta = \frac{P_{\max 1} - P_{\min 1}}{P_{\max 1} + P_{\min 1}}. \tag{12}$$

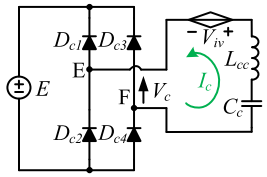

Fig. 4. Controlled source equivalent circuit of the clamp loop.

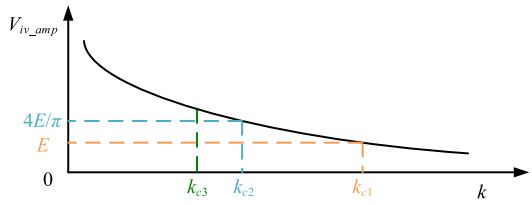

Fig. 5. V_{iv_amp} profile versus the coupling k.

Substituting (12) into (10), $P_{\min 1}$ can be calculated as follows:

$$P_{\min 1} = \frac{V_p^2 (1-\beta)}{2 X_p (1+\beta)}. \tag{13}$$

Substituting (13) into (8), k_{min1} and k_{max1} can be obtained as follows:

$$\begin{cases} k_{\min 1} = \sqrt{\frac{X_p R_{ac}\left(1-\sqrt{\beta}\right)}{\omega^2 L_p L_s\left(1+\sqrt{\beta}\right)}} \\ k_{\max 1} = \sqrt{\frac{X_p R_{ac}\left(1+\sqrt{\beta}\right)}{\omega^2 L_p L_s\left(1-\sqrt{\beta}\right)}} \end{cases}. \tag{14}$$

B. Analysis of the Transformation Process

1) First Critical Coupling Coefficient: Fig. 4 shows the controlled source equivalent circuit of the clamp loop in the clamped IPT system. With the effect of the clamp transformer, the induced voltage V_{iv} generated from the primary loop current, and the corresponding amplitude V_{iv_amp} can be calculated as shown in the following equation:

$$\begin{cases} V_{iv} = j M_c I_p = -\frac{V_p \omega M_c R_{ac}\left(X_p R_{ac} + j L_p L_s \omega^2 k^2\right)}{X_p^2 R_{ac}^2 + L_p^2 L_s^2 \omega^4 k^4} \\ V_{iv\_amp} = \sqrt{2}\,|V_{iv}| = \sqrt{\frac{2 V_p^2 \omega^2 M_c^2 R_{ac}^2}{X_p^2 R_{ac}^2 + L_p^2 L_s^2 \omega^4 k^4}} \end{cases}. \tag{15}$$

Because the clamp loop is in a turn-OFF state, V_{iv} and V_{iv_amp} are also equal to V_c and the corresponding amplitude $V_{c\cdot amp}$. When the IPT system has the misalignment issue, the coupling coefficient k will decrease, and V_{iv_amp} will increase according to (15), which can be drawn in Fig. 5. Once $V_{iv\cdot amp}(V_{c\cdot amp})$ is more than E, the rectifier $(D_{c1} - D_{c4})$ will be activated. Hence, letting $V_{iv\cdot amp} = E$ and combining (3) and (15), the corresponding critical coupling coefficient k_{c1} can be calculated as follows:

$$k_{c1} = \sqrt[4]{\frac{16 M_c^2 R_{ac}^2}{\pi^2 \omega^2 L_p^2 L_s^2} - \frac{X_p^2 R_{ac}^2}{\omega^4 L_p^2 L_s^2}}. \tag{16}$$

2) Second Critical Coupling Coefficient: Assumed that the clamped loop is opportunely fully activated, the relationship

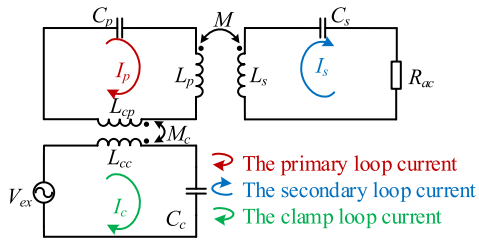

Fig. 6. Equivalent circuit with the external power.

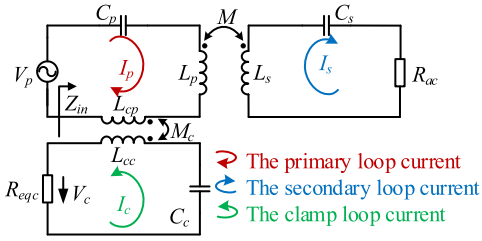

Fig. 7. Simplified circuit.

between E and V_c satisfies

$$V_c = V_p = 2\sqrt{2}E/\pi. \tag{17}$$

And the corresponding amplitude V_{c_amp} can be expressed as follows:

$$V_{c\_amp} = \sqrt{2}V_p = 4E/\pi. \tag{18}$$

Theoretically, under ideal conditions where there are no harmonics in the system, the clamped circuit can be fully activated when $V_{iv\_amp} \geq 4E/\pi$. Substituting (18) into (15), the second critical coupling coefficient k_{c2} can be expressed as follows:

$$k_{c2} = \sqrt[4]{\frac{M_c^2 R_{ac}^2}{\omega^2 L_p^2 L_s^2} - \frac{X_p^2 R_{ac}^2}{\omega^4 L_p^2 L_s^2}}. \tag{19}$$

However, the harmonics are not evitable because of the nonsinusoidal inverter output voltage and rectifier input voltage. Due to the effect of harmonic current [28], [29], the rectifier bridge ($D_{c1} - D_{c4}$) may operate in a discontinuous conduction mode (DCM) even $V_{iv\_amp} \geq 4E/\pi$. Namely, suppose the coupling coefficient k is slightly less than k_{c2} in practice, the clamped circuit may still be partly activated.

3) Third Critical Coupling Coefficient: According to the work in [28] and [29], the boundary of the critical mode between DCM and continuous conduction mode (CCM) can be given as follows:

$$\pi R_{eqcc}/4 = \omega \lim_{m\to\infty} Z_{c(2m+1)}/(2m+1)\,\omega \tag{20}$$

where R_{eqcc} is the critical equivalent ac load of the rectifier constituted by $D_{c1} - D_{c4}$ between DCM and CCM, $Z_{c(2m+1)}$ is the high-frequency output impedance of the clamped IPT system reflected in the clamped circuit, which can be obtained as follows.

Because the output impedance is the same as the Thevenin equivalent at the output terminals, thus, we can simplify the circuit to solve the output impedance based on the external excitation method [30]. First, the independent power should be set to zero, namely the independent square wave voltage source of the primary loop should be short-circuited. Then, we can add an external power V_{ex} to calculate the input impedance at different frequencies ω. Finally, the corresponding equivalent circuit with external power can be described in Fig. 6, which can be described as follows:

$$\begin{cases} 0 = jX_{p(2m+1)}I_p - j(2m+1)\omega M I_s \\ \quad\quad + j(2m+1)\omega M_c I_c \\ 0 = -j(2m+1)\omega M I_p + jX_{s(2m+1)}I_s + R_{ac}I_s \\ V_{ex} = j(2m+1)\omega M_c I_p + jX_{c(2m+1)}I_c \end{cases} \tag{21}$$

where $X_{p(2m+1)}$, $X_{s(2m+1)}$, and $X_{c(2m+1)}$ are the equivalent reactance of each loop when the angular frequency is $(2m+1)\omega$.

Then, $Z_{c(2m+1)}$ can be calculated as given in (22) shown at the bottom of the next page, by solving (21). Substituting (20) into (2), the third critical coupling coefficient k_{c3} can be calculated as (23) shown at the bottom of the next page.

Therefore, when the coupling coefficient k satisfies $k_{c3} < k < k_{c1}$, the clamped circuit is partly activated. In this process, the clamped loop current I_c can be considered a very small value [26]. We can approximatively regard the system as a detuned S-S topology.

C. Analysis of Fully Activated Mode

When $k \leq k_{c3}$, the clamped circuit is fully activated, and the system can be simplified as shown in Fig. 7. Combining (2) and (17), the system can be rewritten as

$$\begin{cases} V_p = jX_p I_p - j\omega M I_s + j\omega M_c I_c \\ V_s = R_{ac}I_s = j\omega M I_p - jX_s I_s \\ V_p = R_{eqc}I_c = j\omega M_c I_p + jX_c I_c \end{cases}. \tag{24}$$

Similarly, substituting $X_s = 0$ into (24), the input impedance, the input impedance angle, and the output power can be obtained as follows:

$$\begin{cases} Z_{in} = \frac{V_p}{I_p} = \frac{L_p L_s \omega^2 k^2}{R_{ac}} + \frac{\omega^2 M_c^2 (R_{eqc} - jX_c)}{X_c^2 + R_{eqc}^2} + jX_p \\ \theta = \arctan\left(\frac{R_{ac}\left(X_p X_c^2 + X_p R_{eqc}^2 - \omega^2 M_c^2 X_c\right)}{L_p L_s \omega^2 k^2 \left(X_c^2 + R_{eqc}^2\right) + R_{ac} R_{eqc} \omega^2 M_c^2} \right) \end{cases} \tag{25}$$

$$\begin{aligned} P_{o2}(k) &= |I_s|^2 R_{ac} \\ &= \frac{V_p^2 R_{ac} L_p L_s \omega^2 k^2 (X_c - \omega M_c)^2}{R_{ac}^2 (X_p X_c - \omega^2 M_c^2)^2 + L_p^2 L_s^2 \omega^4 k^4 X_c^2}. \end{aligned} \tag{26}$$

From (26), the variation tendency of the output power P_{o2} is similar to P_{o1}, which can be depicted in Fig. 8 to distinguish P_{o1}. Setting the derivative of P_{o2} to zero, the maximum output power $P_{\max 2}$ and the corresponding coupling coefficient k_{pmax2}

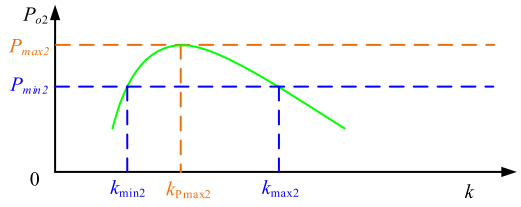

Fig. 8. Curve of the output power P_{o2} in the fully activated mode, where $P_{\max 2}$ is the maximum output power, k_{pmax2} is the corresponding coupling coefficient, $P_{\min 2}$ is presumed minimum output power, and the corresponding couplings are $k_{\min 2}$ and $k_{\max 2}$.

can be calculated as follows:

$$\begin{cases} k_{p\max 2} = \sqrt{\frac{R_{ac}(X_pX_c-\omega^2M_c^2)}{\omega^2X_cL_pL_s}} \\ P_{\max 2} = \frac{V_p^2(X_c-\omega M_c)^2}{2X_pX_c^2-2X_c\omega^2M_c^2} \end{cases}. \tag{27}$$

Moreover, the presumed minimum output power $P_{\min 2}$ satisfies

$$P_{\min 2} = P_{o2}\left(k_{\min 2}\right) = P_{o2}\left(k_{\max 2}\right). \tag{28}$$

Then, β also can be employed to describe the power fluctuation in this case, namely

$$\beta = \frac{P_{\max 2} - P_{\min 2}}{P_{\max 2} + P_{\min 2}}. \tag{29}$$

Similarly, $P_{\min 2}$, $k_{\min 2}$, and $k_{\max 2}$ can be calculated as follows:

$$\begin{cases} P_{\min 2} = \frac{V_p^2(1-\beta)(X_c-\omega M_c)^2}{2(1+\beta)(X_pX_c^2-X_c\omega^2M_c^2)} \\ k_{\min 2} = \sqrt{\frac{R_{ac}(X_pX_c-\omega^2M_c^2)\left(1-\sqrt{\beta}\right)}{\omega^2L_pL_sX_c\left(1+\sqrt{\beta}\right)}} \\ k_{\max 2} = \sqrt{\frac{R_{ac}(X_pX_c-\omega^2M_c^2)\left(1+\sqrt{\beta}\right)}{\omega^2L_pL_sX_c\left(1-\sqrt{\beta}\right)}} \end{cases}. \tag{30}$$

Compared with the traditional detuned circuit, the proposed IPT system has two maximum power points according to (10) and (27), i.e., $P_{\max 1}$ and $P_{\max 2}$. If the parameters are reasonably designed, the two top power points can be employed so that the system has a wide coupling range with stable output power in misalignment conditions.

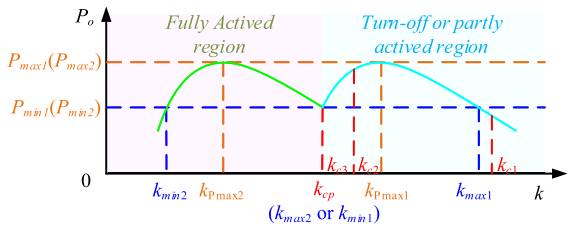

Fig. 9. Output power curve versus coupling.

III. System Design

A. Circuit Parameters Design

In order to achieve stable power transfer versus a large coupling variation, the output power curves of the two modes should overlap at the minimum output power $P_{\min}$, as shown in Fig. 9. For readability, a variable k_{cp} is used to express the coupling coefficient of the coincidence point. Ideally, the maximum output power should be the same in the two modes. Then, the constraints can be concluded as follows [21]:

$$\begin{cases} k_{\min 1} = k_{\max 2} = k_{cp} \\ P_{\max 1} = P_{\max 2} \\ P_{\min 1} = P_{\min 2} \end{cases}. \tag{31}$$

Substituting (10), (13), (14), (27), and (30) into (31), the constraints can be rewritten as follows:

$$\begin{cases} \sqrt{\frac{X_pR_{ac}\left(1-\sqrt{\beta}\right)}{\omega^2L_pL_s\left(1+\sqrt{\beta}\right)}} = k_{cp} \\ \sqrt{\frac{R_{ac}(X_pX_c-\omega^2M_c^2)\left(1+\sqrt{\beta}\right)}{\omega^2L_pL_sX_c\left(1-\sqrt{\beta}\right)}} = k_{cp} \\ \frac{X_pX_c^2-X_c\omega^2M_c^2}{X_p(X_c-\omega M_c)^2} = 1 \end{cases}. \tag{32}$$

Solving (32), X_p, X_c, and M_c can be calculated as follows:

$$\begin{cases} X_p = \frac{L_pL_s\omega^2k_{cp}^2\left(1+\sqrt{\beta}\right)}{R_{ac}\left(1-\sqrt{\beta}\right)} \\ X_c = \frac{L_pL_s\omega^2k_{cp}^2(1-\beta)}{R_{ac}\sqrt{\beta}\left(1-\sqrt{\beta}\right)^2} \\ M_c = \frac{2L_pL_s\omega k_{cp}^2}{R_{ac}\left(1-\sqrt{\beta}\right)} \end{cases}. \tag{33}$$

$$Z_{c(2m+1)} = \frac{V_{ex}}{I_c} = jX_{c(2m+1)} + \frac{(2m+1)^2\omega^2M_c^2\left((2m+1)^2\omega^2k^2L_pL_s\left(R_{ac}+jX_{s(2m+1)}\right) - jX_{p(2m+1)}R_{ac}^2 - jX_{p(2m+1)}X_{s(2m+1)}^2\right)}{\left(X_{p(2m+1)}X_{s(2m+1)} - (2m+1)^2\omega^2k^2L_pL_s\right)^2 + X_{p(2m+1)}R_{ac}^2} \tag{22}$$

$$k_{c3} = \sqrt{\frac{R_{ac}\left(\sqrt{\left(X_c^2+R_{eqcc}^2\right)\left(\omega^2M_c^2R_{eqcc}^2-X_p^2X_c^2\right)} - \left(X_pR_{eqcc}^2-\omega^2M_c^2X_c\right)^2 + X_pX_c^2\left(2X_c\omega^2M_c^2-X_pR_{eqcc}^2\right) - \omega^2M_c^2R_{eqcc}\right)}{L_pL_s\omega^2\left(X_c^2+R_{eqcc}^2\right)}} \tag{23}$$

TABLE I
PARAMETER VALUES

Parameter	Value	Parameter	Value
ω	2×π×250 kHz	R	20 Ω
β	5.6%	k_{cp}	0.25
L_p	48.87 μH	L_s	45.77 μH
X_p	34.47 Ω	X_c	145.66 Ω
M_c	35.49 μH		

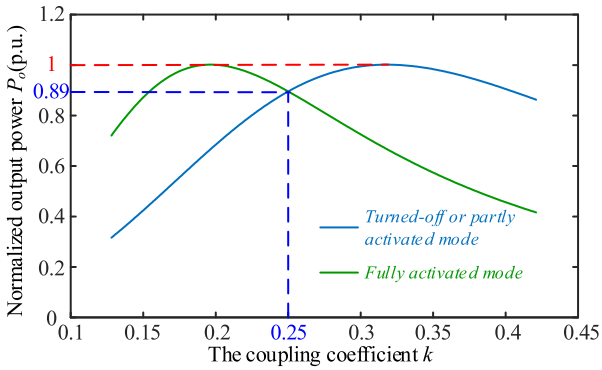

Fig. 10. Theoretical transfer power curve.

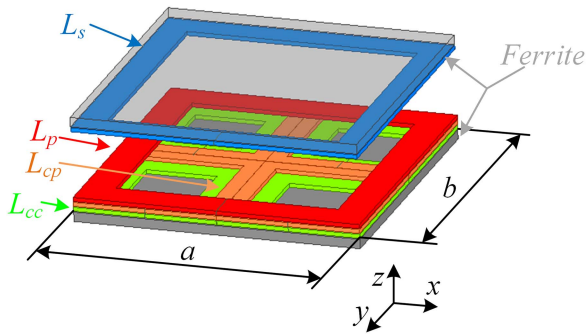

Fig. 11. Magnetic coupler using QDQP structure.

As an example, we can substitute the parameters listed in Table I into (33), X_p, X_c, and M_c can be calculated and the corresponding results are listed in Table I. Substituting the parameters of Table I into (8) and (26), the transfer power can be depicted as Fig. 10. The power curves accord with our expectations.

Through the above circuit parameter design method, we can create the desired power curve. However, the transition between the different modes is still uncertain. According to the analysis of Section II, the conversion between the two modes depends on k_{c3}. Hence, k_{cp} should be equal to k_{c3} so that one mode can be smoothly switched to another, as Fig. 9. From (20) to (23), k_{c3} is related to all circuit parameters. Thus, we can design the clamp transformer to make k_{c3} reach the predetermined value.

B. Coupled Structure Design

To eliminate the coupling between the clamp loop and the secondary side loop, a quadruple D quadrate pad (QDQP) [12], [31], [32] is adopted, as shown in Fig. 11. It is noted that the stand-alone inductor has almost identical electrical performance

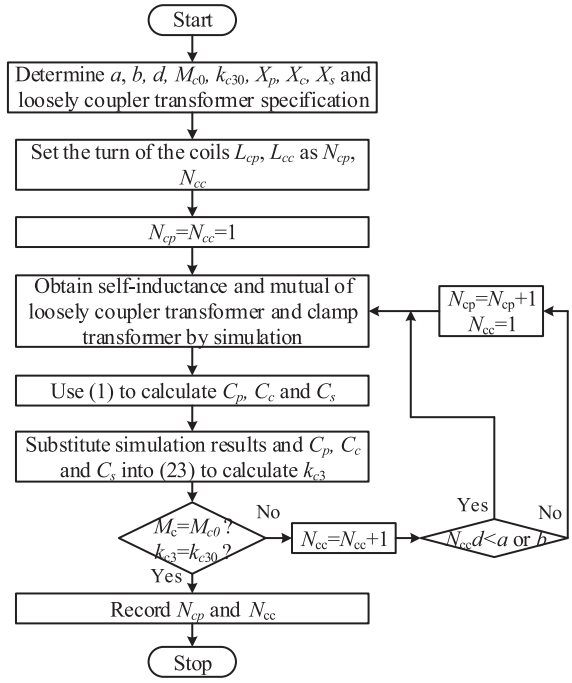

Fig. 12. Flowchart for the design of clamp transformer, where a and b are length and width, d is Litz wire diameter, M_{c0} and k_{c30} are the predetermined mutual inductance of clamp transformer and critical coupling coefficient of the loosely coupled transformer.

as the integrated inductor [31]. Hence, a tightly coupled transformer can also be used to form a clamp transformer [33]. However, the hardware volume is increased inevitably. Thus, this work uses a compact magnetic coupler scheme, i.e., QDQP structure. Similar to the coil structure of the conventional IPT system, two quadrate pads (QP) are placed on the primary and secondary sides to form the loosely coupled transformer. The difference is that two quadruple D pads (QDP) on the primary and clamp loop form the clamp transformer. Hence, the magnetic design of this work is focused on the clamp transformer. For the QDP, the direction of the current in the adjacent coils should be opposite to create the orthogonal magnetic flux with QP [12]. Due to the symmetrical, the magnetic flux passing from QDP (QP) to QP (QDP) is zero in ideal conditions, so the loosely coupled transformer and clamp transformer can be decoupled.

After obtaining the design value of M_c, the clamp coil can be designed to meet the requirements of the mutual inductor while adjusting the self-inductance of the clamp coil so that k_{c3} reaches the preset value. The detailed design procedures are given in Fig. 12. First, we can predetermine the length a and width b of clamp coils, the Litz wire diameter d, the mutual inductance M_{c0} of clamp transformer, the third critical coupling coefficient k_{c30}, the primary loop equivalent reactance X_p, the clamp loop equivalent reactance X_c, the secondary loop equivalent reactance X_s, and loosely coupled transformer specification. Then, the turn of clamp coils is initialized. Next, we can obtain the coil parameters (self-inductance and mutual) of the loosely coupled transformer and clamp transformer by Maxwell. Subsequently, C_p, C_c, and C_s can be calculated according to (1). Next, the third critical

TABLE II
COILS' SELF-INDUCTANCES AND CAPACITOR

Parameter	Design value	Parameter	Design value
L_p	48.87 μH	L_s	45.77 μH
L_{cc}	98.47 μH	L_{cp}	27.33 μH
C_p	7.47 nF	C_c	70.06 nF
C_s	8.85 nF		

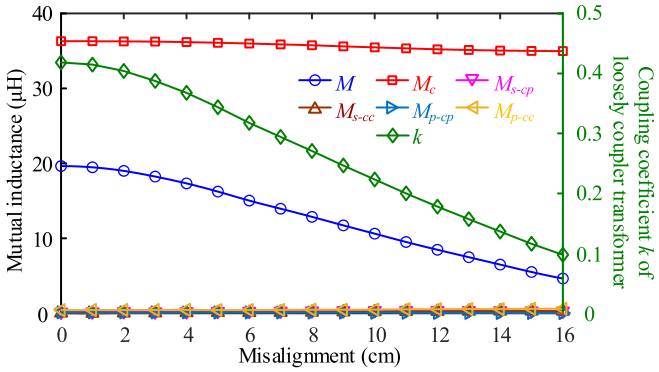

Fig. 13. Mutual inductance between coils with x-misalignment.

coupling can be calculated by substituting simulation results and C_p, C_c, and C_s into (23). Finally, the mutual inductance of the clamp transformer and the third critical coupling can be evaluated to determine whether they are equal to the preset value M_{c0} and k_{c30}. If yes, the turn of clamp coils will be recorded. Otherwise, the turn of clamp coils will be regulated to repeat the above procedures.

As an example, the length and width of the clamp transformer are set to be the same as the loosely coupled transformer, namely $a = b = 300$ mm. Besides, according to the design results of circuit parameters, M_{c0} and k_{c30} are designed as 35.49 μH and 0.25, X_p, X_c, and X_s are defined as 34.47, 145.66, and 0 Ω. As a result, N_{cp} and N_{cc} are iterated as 4 and 9, respectively. Then, the measured coils' self-inductances and the calculated capacitor are given in Table II. And the mutual inductance is depicted in Fig. 13 with x-misalignment. It is obvious that the mutual inductance (M) and the coupling coefficient (k) of the loosely coupled transformer have large variations with misalignments, while the mutual inductance (M_c) of the clamp transformer is almost constant. Besides, the cross-couplings ($M_{p\text{-}cp}$, $M_{p\text{-}cc}$, $M_{s\text{-}cp}$, and $M_{s\text{-}cc}$) between the loosely coupled transformer and clamp transformer are very small and can be ignored. The results of xy-misalignment are offered in Fig. 14. The variation trends of M, k, M_c, $M_{p\text{-}cp}$, and $M_{p\text{-}cc}$ are similar to x-misalignment, while the cross-couplings ($M_{s\text{-}cp}$ and $M_{s\text{-}cc}$) between clamp coils (L_{cc} and L_{cp}) and the secondary coil (L_s) cannot be neglected once the diagonal misalignment is larger than 5 cm, which may affect the misalignment performance.

IV. EXPERIMENTAL RESULTS

To demonstrate the validity of the proposed method, a 480 W experimental prototype was built, as shown in Fig. 15(a). The coils structure is given in Fig. 15(b), where the quadruple-D

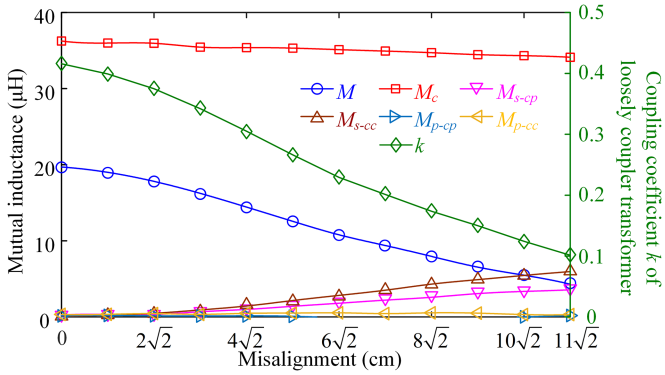

Fig. 14. Mutual inductance between coils with xy-misalignment.

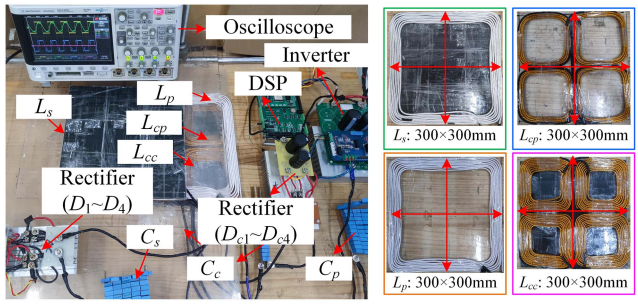

Fig. 15. Experimental prototype. (a) Overall setup. (b) Coils structure.

TABLE III
PARAMETER VALUES

Parameter	Value	Parameter	Value
E	230 V	ω	2×π×250 kHz
L_p	48.87 μH	L_s	45.77 μH
L_{cc}	98.47 μH	L_{cp}	27.33 μH
M_c	35.49 μH	C_p	7.73 nF
C_c	70.17 nF	C_s	9.02 nF
k_{c3}	0.25	R	20 Ω
R_{Cp}	12 mΩ	R_{Cs}	21 mΩ
R_{Cc}	18 mΩ	R_{Lp}	102 mΩ
R_{Lcp}	57 mΩ	R_{Ls}	114 mΩ
R_{Lcc}	172 mΩ		

TABLE IV
DEVICE'S MODELS

Device	Model
DC power source	Chroma 62150H-600
MOSFETs Q_1-Q_4	C2M0080120D
Rectifier diodes D_1-D_4	DSEI2×61−06C
Clamp diodes D_{c1}-D_{c2}	DSEI2×61−06C
Electronic load	ITECH IT8816B

quadrature pads are used as the clamp transformer to eliminate the cross-coupling with the loosely coupled transformer [12]. According to the proposed parameter design method, a set of parameters are listed in Table III, and the corresponding devices are given in Table IV.

The transfer power and efficiency against coupling variation are given in Fig. 16. The output power is depicted in Fig. 16(a).

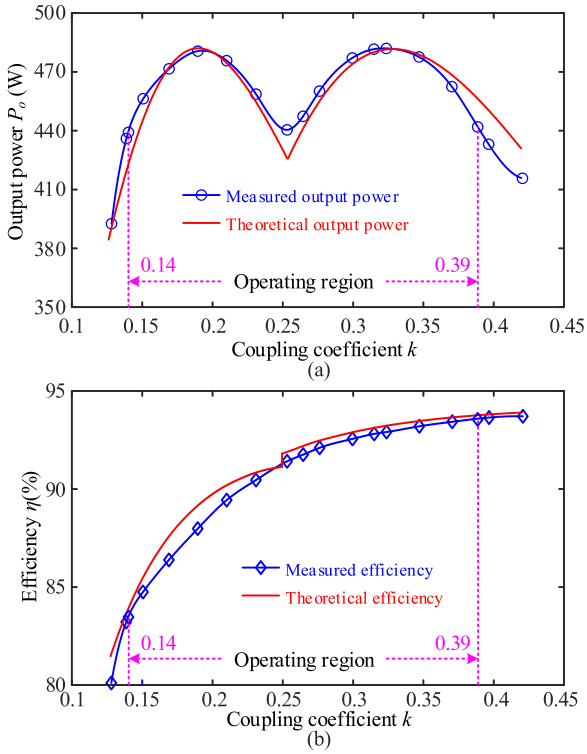

Fig. 16. Experimental and theoretical results of (a) output power and (b) efficiency with x-misalignment.

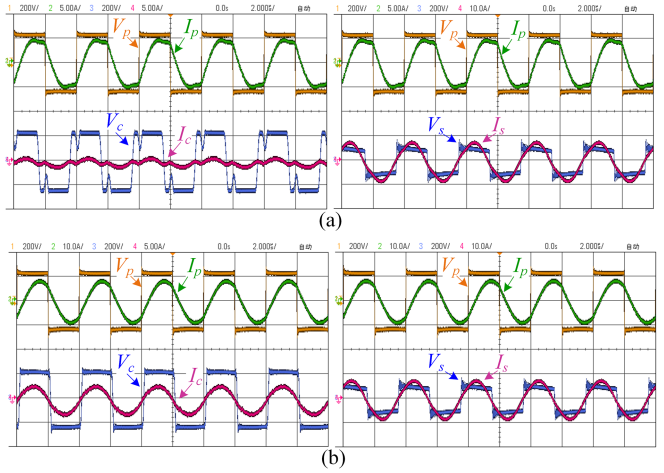

Fig. 17. Waveforms of the inverter output and the input of the rectifier at (a) $k = 0.32$ and (b) $k = 0.19$.

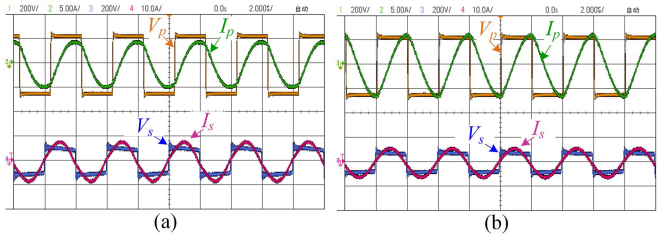

Fig. 18. Measured waveforms of the inverter output and the input of the rectifier for the IPT system without the clamping circuit at (a) $k = 0.32$ and (b) $k = 0.19$.

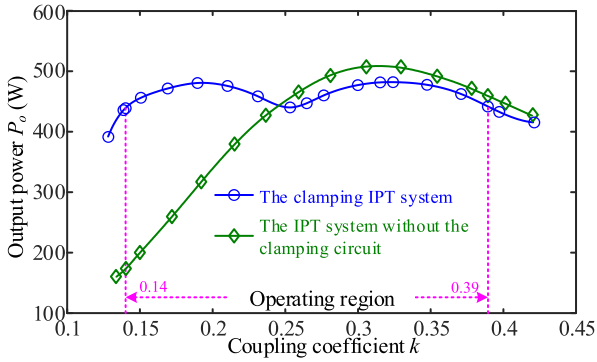

Fig. 19. Measured output power of the clamped IPT system and the IPT system without the clamping circuit.

It can be seen that the output power varies between 440 and 480 W with the coupling k decreasing from 0.39 to 0.14. The fluctuation of power is only 4.3%, which can be calculated by $(P_{max} - P_{\min})/(P_{\max} + P_{\min})$. Additionally, the efficiency is drawn in Fig. 16(b), which decreases from 93.55% to 83.22% within the coupling range [0.14, 0.39]. The efficiency decline is mainly attributed to the reduction of coupling and the extra power loss due to the clamp circuit. The theoretical prediction of the output power and the efficiency are also given in Fig. 16. The maximum error of the output power is 15 W when k is 0.25, while that of the efficiency is 1.27% when k is equal to 0.19. Meanwhile, the error is inevitable, and it mainly comes from the deviation of the parameters, the resistance of each reactive element, and the insufficient accuracy of the fundamental approximation method in the partly activated mode of the clamp circuit [26]. Nevertheless, the results still are acceptable.

The experimental waveforms at the two maximum power points are displayed in Fig. 17. When the system works in turned-OFF or partly activated mode, the clamp loop current is small, so the system can be approximatively regarded as the detuned SS topology, as shown in Fig. 17(a). Besides, I_c is distorted due to the harmonic current, leading to the rectifier $(D_{c1} - D_{c4})$ operating in a DCM [28], [29]. With the coupling decrease, the system enters the fully activated mode, as Fig. 17(b). In this case, the rectifier $(D_{c1} - D_{c4})$ is fully conducted, and the clamp loop current cannot be ignored. With the effect of the clamp circuit, the output power still maintains stable from Fig. 16. Besides, V_s and I_s have almost the same amplitude according to Fig. 17(a) and (b), which verifies the validity of the proposed method.

To show the effectiveness of the proposed method, the clamp circuit is removed. The system can be regarded as the detuned S-S topology [7]. Fig. 18 shows the waveforms of the system without the clamping circuit when the coupling is 0.32 and 0.19. We can see that the output voltage V_s and current I_s are significantly reduced with the decrease of the coupling. The output power is measured in Fig. 19. According to the measured results, the power is slightly lower than the IPT system without the clamping circuit when the clamping IPT system works in turned-OFF or partly activated mode, namely the coupling decreases from 0.39 to 0.25. The main reason is the insufficient

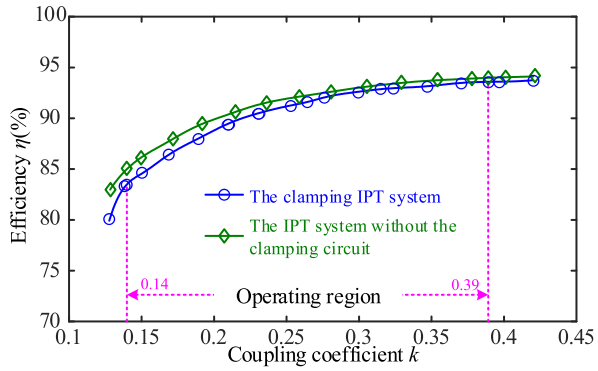

Fig. 20. Measured efficiency of the clamped IPT system and the IPT system without the clamping circuit.

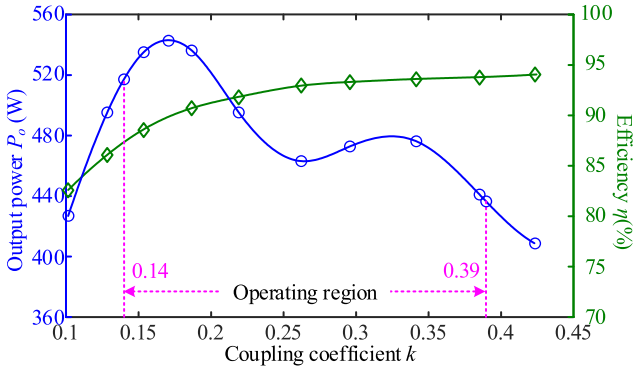

Fig. 22. Measured output power and efficiency with xy-misalignment.

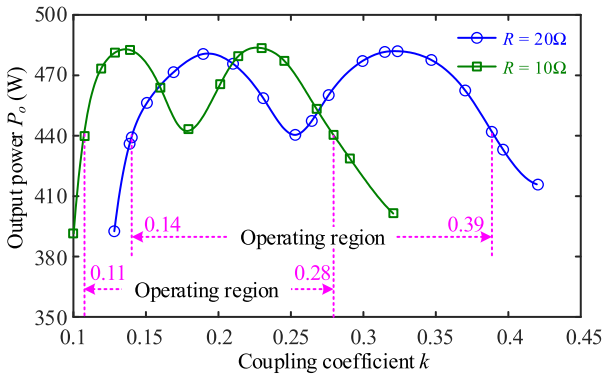

Fig. 21. Output power with different loads.

accuracy of the fundamental approximation method in the partly activated mode of the clamp circuit [26]. With further reduction of the coupling, the power of the IPT system without the clamp circuit declines significantly, while the proposed method output power still is stable. In terms of the overall power variation, the output power of the IPT system without the clamping circuit is between 210 and 505 W when coupling varies from 0.14 to 0.39, and the power fluctuation is 41.26%, which is inferior to the proposed method (4.3%). Moreover, the system efficiency is measured in Fig. 20. Similarly, the efficiency varies from 85.12% to 94.14%, with the coupling increasing from 0.14 to 0.39. Due to the power loss in the clamp circuit, the efficiency of the IPT system without the clamping circuit is slightly higher than that of the proposed method.

When the load is changed, $P_{\max}$ and $P_{\min}$ are constant with the load variation based on (10), (13), (27), and (30), while k_{c1}, k_{c2}, k_{c3}, k_{pmax1}, k_{pmax2}, $k_{\min 1}$, $k_{\max 1}$, $k_{\min 2}$, and $k_{\max 2}$ are changed concurrently in the same proportion according to (9), (14), (16), (19), (23), (27), and (30). Fig. 21 shows the output power with the different loads. It can be seen the output power moves to the left when the load decreases from 20 to 10 Ω. Besides, the load variation hardly affects the maximum and minimum output power, but the coupling range with stable power transfer is varied. Hence, the load is better fixed if the system is required to operate within the determined coupling range.

When the secondary side has a xy-misalignment, the results are measured in Fig. 22. With the coupling decrease, the output power deviates from the expected value (480 W) when the coupling is lower than 0.23. The maximum output power reaches 540 W, and the power fluctuation is larger than 10% due to the cross-couplings ($M_{s\text{-}cp}$ and $M_{s\text{-}cc}$). It is noted that the stand-alone inductor has almost identical electrical performance as the integrated inductor [31]. Hence, a tightly coupled transformer can also be used to form the clamp transformer to avoid the effects of cross-coupling by compromising the hardware volume in theory [33].

V. Conclusion

A detuned SS-compensated IPT system with a clamped circuit is proposed to improve misalignment tolerance versus the wide coupling variation. Wireless feedback communication or closed-loop control is not required for the proposed method. The operating principle and misalignment characteristics are analyzed in detail. And then, circuit parameters are optimized to obtain high-misalignment tolerance. With the proposed parameter design method, an IPT system was built. Experimental results show that the power fluctuation is only 4.4%, and the maximum efficiency can reach 93.55% with 278.6% coupling variation (0.14–0.39), verifying the feasibility of the proposed method.

References

[1] X. Qing, Y. Su, A. P. Hu, X. Dai, and Z. Liu, "Dual-loop control method for CPT system under coupling misalignments and load variations," *IEEE J. Emerg. Sel. Topics Power Electron.*, vol. 10, no. 4, pp. 4902–4912, Aug. 2022.

[2] Z. Li, H. Liu, Y. Huo, J. He, Y. Tian, and J. Liu, "High-misalignment tolerance wireless charging system for constant power output using dual transmission channels with magnetic flux controlled inductors," *IEEE Trans. Power Electron.*, vol. 37, no. 11, pp. 13930–13945, Nov. 2022.

[3] Z. Zhang, F. Zhu, D. Xu, P. T. Krein, and H. Ma, "An integrated inductive power transfer system design with a variable inductor for misalignment tolerance and battery charging applications," *IEEE Trans. Power Electron.*, vol. 35, no. 11, pp. 11544–11556, Nov. 2020.

[4] Z. Zhang, F. Zhu, D. Xu, P. T. Krein, and H. Ma, "An integrated inductive power transfer system design with a variable inductor for misalignment tolerance and battery charging applications," *IEEE Trans. Power Electron.*, vol. 35, no. 11, pp. 11544–11556, Nov. 2020.

[5] Z. Li, H. Liu, Y. Huo, J. He, Y. Tian, and J. Liu, "High-misalignment tolerance wireless charging system for constant power output using dual transmission channels with magnetic flux controlled inductors," *IEEE Trans. Power Electron.*, vol. 37, no. 11, pp. 13930–13945, Nov. 2022.
[6] H. Feng, T. Cai, S. Duan, X. Zhang, H. Hu, and J. Niu, "A dual-side-detuned series–series compensated resonant converter for wide charging region in a wireless power transfer system," *IEEE Trans. Ind. Electron.*, vol. 65, no. 3, pp. 2177–2188, Mar. 2018.
[7] Y. Liu, U. K. Madawala, R. Mai, and Z. He, "An optimal multivariable control strategy for inductive power transfer systems to improve efficiency," *IEEE Trans. Power Electron.*, vol. 35, no. 9, pp. 8998–9010, Sep. 2020.
[8] Y. Yao, Y. Wang, X. Liu, Y. Pei, and D. Xu, "A novel unsymmetrical coupling structure based on concentrated magnetic flux for high-misalignment IPT applications," *IEEE Trans. Power Electron.*, vol. 34, no. 4, pp. 3110–3123, Apr. 2019.
[9] Y. Chen, R. Mai, Y. Zhang, M. Li, and Z. He, "Improving misalignment tolerance for IPT system using a third-coil," *IEEE Trans. Power Electron.*, vol. 34, no. 4, pp. 3009–3013, Apr. 2019.
[10] G. Yang et al., "Interoperability improvement for rectangular pad and DD pad of wireless electric vehicle charging system based on adaptive position adjustment," *IEEE Trans. Ind. Appl.*, vol. 57, no. 3, pp. 2613–2624, May/Jun. 2021.
[11] L. Zhao, D. J. Thrimawithana, U. K. Madawala, A. P. Hu, and C. C. Mi, "A misalignment-tolerant series-hybrid wireless EV charging system with integrated magnetics," *IEEE Trans. Power Electron.*, vol. 34, no. 2, pp. 1276–1285, Feb. 2019.
[12] Y. Chen et al., "A hybrid inductive power transfer system with misalignment tolerance using quadruple-D quadrature pads," *IEEE Trans. Power Electron.*, vol. 35, no. 6, pp. 6039–6049, Jun. 2020.
[13] R. Mai, B. Yang, Y. Chen, N. Yang, Z. He, and S. Gao, "A misalignment tolerant IPT system with intermediate coils for constant-current output," *IEEE Trans. Power Electron.*, vol. 34, no. 8, pp. 7151–7155, Aug. 2019.
[14] X. Qu, Y. Yao, D. Wang, S.-C. Wong, and C. K. Tse, "A family of hybrid IPT topologies with near load-independent output and high tolerance to pad misalignment," *IEEE Trans. Power Electron.*, vol. 35, no. 7, pp. 6867–6877, Jul. 2020.
[15] Y. Yao, Y. Wang, X. Liu, K. Lu, and D. Xu, "Analysis and design of an S/SP compensated IPT system to minimize output voltage fluctuation versus coupling coefficient and load variation," *IEEE Trans. Veh. Technol.*, vol. 67, no. 10, pp. 9262–9272, Oct. 2018.
[16] H. Feng, T. Cai, S. Duan, J. Zhao, X. Zhang, and C. Chen, "An LCC-compensated resonant converter optimized for robust reaction to large coupling variation in dynamic wireless power transfer," *IEEE Trans. Ind. Electron.*, vol. 63, no. 10, pp. 6591–6601, Oct. 2016.
[17] Y. Yao, Y. Wang, X. Liu, Y. Pei, D. Xu, and X. Liu, "Particle swarm optimization-based parameter design method for S/CLC-compensated IPT systems featuring high tolerance to misalignment and load variation," *IEEE Trans. Power Electron.*, vol. 34, no. 6, pp. 5268–5282, Jun. 2019.
[18] W. Chen, W. Lu, H. H.-C. Iu, and T. Fernando, "Compensation network optimal design based on evolutionary algorithm for inductive power transfer system," *IEEE Trans. Circuits Syst. I: Regular Papers*, vol. 67, no. 12, pp. 5664–5674, Dec. 2020.
[19] H. Feng, A. Dayerizadeh, and S. M. Lukic, "A coupling-insensitive X-type IPT system for high position tolerance," *IEEE Trans. Ind. Electron.*, vol. 68, no. 8, pp. 6917–6926, Aug. 2021.
[20] J. Mai, Y. Wang, Y. Yao, and D. Xu, "Analysis and design of high-misalignment-tolerant compensation topologies with constant-current or constant-voltage output for IPT systems," *IEEE Trans. Power Electron.*, vol. 36, no. 3, pp. 2685–2695, Mar. 2021.
[21] Y. Chen et al., "Reconfigurable topology for IPT system maintaining stable transmission power over large coupling variation," *IEEE Trans. Power Electron.*, vol. 35, no. 5, pp. 4915–4924, May 2020.
[22] G. Lee, B. H. Waters, Y. G. Shin, J. R. Smith, and W. S. Park, "A reconfigurable resonant coil for range adaptation wireless power transfer," *IEEE Trans. Microw. Theory Techn.*, vol. 64, no. 2, pp. 624–632, Feb. 2016.
[23] Y. Zhang et al., "Misalignment-tolerant dual-transmitter electric vehicle wireless charging system with reconfigurable topologies," *IEEE Trans. Power Electron.*, vol. 37, no. 8, pp. 8816–8819, Aug. 2022.
[24] Y. Chen, S. He, B. Yang, S. Chen, Z. He, and R. Mai, "Reconfigurable rectifier-based detuned series-series compensated IPT system for anti-misalignment and efficiency improvement," *IEEE Trans. Power Electron.*, vol. 38, no. 2, pp. 2720–2729, Feb. 2023.
[25] H.-C. Hsieh and J.-S. Lai, "A half-bridge CLC-series wireless power transfer system with clamping diodes," in *Proc. IEEE Int. Future Energy Electron. Conf.*, 2021, pp. 1–6.
[26] Z. Huang, G. Wang, J. Yu, and X. Qu, "A novel clamp coil assisted IPT battery charger with inherent CC-to-CV transition capability," *IEEE Trans. Power Electron.*, vol. 36, no. 8, pp. 8607–8611, Aug. 2021.
[27] P. Cao et al., "An IPT system with constant current and constant voltage output features for EV charging," in *Proc. 44th Annu. Conf. IEEE Ind. Electron. Soc.*, 2018, pp. 4775–4780.
[28] W. Li, Q. Zhang, H. Li, C. Cui, and G. Wei, "Series filter computational method for CCM recovery in double side LCC WPT system," *IEEE Trans. Ind. Electron.*, vol. 69, no. 9, pp. 8875–8882, Sep. 2022.
[29] J. Mai, X. Zeng, Y. Yao, Y. Wang, and D. Xu, "Impedance analysis and design of IPT system to improve system efficiency and reduce output voltage or current fluctuations," *IEEE Trans. Power Electron.*, vol. 36, no. 12, pp. 14029–14038, Dec. 2021.
[30] C. K. Alexander and M. N. O. Sadiku. *Fundamentals of Electric Circuits, Chapter 19 Two-Port Networks*, 4th ed. New York, NY, USA: McGraw-Hill, 2008.
[31] S. Chen, Y. Chen, N. A. Dung, R. Mai, and Y. Tang, "A compact wireless charger design with decoupled quadruple-D inductor for LCC-series topologies," in *Proc. IEEE 4th Int. Future Energy Electron. Conf.*, 2019, pp. 1–7.
[32] A. Ahmad, M. S. Alam, and A. A. S. Mohamed, "Design and interoperability analysis of quadruple pad structure for electric vehicle wireless charging application," *IEEE Trans. Transp. Electrific.*, vol. 5, no. 4, pp. 934–945, Dec. 2019.
[33] R. Mai, P. Yue, Y. Liu, Y. Zhang, and Z. He, "A dynamic tuning method utilizing inductor paralleled with load for inductive power transfer," *IEEE Trans. Power Electron.*, vol. 33, no. 12, pp. 10924–10934, Dec. 2018.

Bin Yang (Student Member, IEEE) received the B.S. degree in electrical engineering and automation from the School of Electrical and Automation Engineering, East China Jiaotong University, Nanchang, China, in 2017. He is currently working toward the Ph.D. degree in electrical engineering with the School of Electrical Engineering, Southwest Jiaotong University, Chengdu, China.

His main research interest focuses on wireless power transfer, especially on misalignment tolerance improvement.

Binshan Zhang received the B.S. degree in electrical engineering and automation from the School of Electrical Engineering, Chongqing Metropolitan College of Science and Technology, Chongqing, China, in 2020. He is currently working toward the B.Sc. degree in electrical engineering with the School of Electrical Engineering, Southwest Jiaotong University, Chengdu, China.

His main research interest focuses on wireless power transfer.

Zeheng Zhang received the B.S. degree in electrical engineering and automation from the School of Electrical Engineering, Ji'nan University, Zhuhai, China, in 2022. He is currently working toward the B.Sc. degree in electrical engineering with the School of Electrical Engineering, Southwest Jiaotong University, Chengdu, China.

His research interest focuses on wireless power transfer.

Ying Luo received the B.Sc. degree in electrical engineering and automation in 2017 from the School of Electrical Engineering, Southwest Jiaotong University, Chengdu, China, where she is currently working toward the Ph.D. degree in electrical engineering.

Her main research interest focuses on wireless power transfer.

Ruikun Mai (Senior Member, IEEE) received the B.Sc. and Ph.D. degrees in electrical engineering from the School of Electrical Engineering, Southwest Jiaotong University, Chengdu, China, in 2004 and 2010, respectively.

He is currently a Professor with the School of Electrical Engineering, Southwest Jiaotong University. His research interests include wireless power transfer and its application in railway systems, power system stability and control.

Zhengyou He (Senior Member, IEEE) received the B.Sc. and M.Sc. degrees in computational mechanics from Chongqing University, Chongqing, China, in 1992 and 1995, respectively, and the Ph.D. degree in electrical engineering from the School of Electrical Engineering, Southwest Jiaotong University, Chengdu, China, in 2001.

He is currently a Professor with the School of Electrical Engineering, Southwest Jiaotong University. His research interests include signal process and information theory applied to electrical power system, and application of wavelet transforms in power system.

Yang Chen (Member, IEEE) received the B.Sc. degree in electrical engineering and automation and the Ph.D. degree in electrical engineering from Southwest Jiaotong University, Chengdu, China, in 2015 and 2020, respectively.

From December 2018 to December 2019, he was a joint Ph.D. student founded by the China Scholarship Council with the Future Energy Electronics Center, Virginia Tech, Blacksburg, VA, USA. He is currently a Postdoctoral Researcher with Southwest Jiaotong University. His research interest focuses on wireless power transfer.